Supplementary Information

Water vapour induced reversible switching between a 1-D coordination polymer and a 0-D aqua complex

Min Deng,[a,‡] Soumya Mukherjee,[b,‡] Yu-Jie Liang,[a] Xiao-Dan Fang,[a] Ai-Xin Zhu*[a] and Michael J. Zaworotko*[b]

[a] Faculty of Chemistry and Chemical Engineering, Yunnan Normal University, Kunming 650500, China.

[b] Department of Chemical Sciences, Bernal Institute, University of Limerick, Limerick V94 T9PX, Republic of Ireland.

*Corresponding authors: zaxchem@126.com; xtal@ul.ie.

‡ M.D. and S.M. contributed equally to this work.

Table of Contents

1. **Materials and synthesis**
2. **Single-crystal X-ray diffraction measurements.**
3. **Single-crystal data and structural parameters**
4. **Additional structure figures**
5. **Summary tables of structural differences among 1α, 1β and 2**
6. **Summary tables of weak interactions in 1α, 1β and 2**
7. **Powder X-ray diffraction (PXRD)**
8. **Thermogravimetric analysis (TGA)**
9. **IR spectra**
10. **Gas and vapor adsorption**
11. **Summary of MOMs with type F-IV water adsorption isotherms**

1. Materials and synthesis

All the chemicals obtained from commercial sources and used without further purification. The ligand 3-(4*H*-1,2,4-triazol-4-yl) benzoic acid (3-Htba) was synthesized according to the literature method.[1]

Synthesis of [Zn(3-tba)$_2$]·DMA (1α). A mixture of $Zn(NO_3)_2 \cdot 6H_2O$ (60 mg, 0.2 mmol), 3-Htba (76 mg, 0.4 mmol), DMA (*N*,*N*′-dimethylacetamide) (8 mL), toluene (1.5 mL) and NaOH (100 uL, 1 mol/L) was placed in a 20 mL vial container. Then heated in an oven at 105 °C for 24 h and then cooled to room temperature at a rate of 5 °C/h. Colourless diamond-shaped crystals of **1α** was collected by filtration, washed with DMA and dried in air to afford 55 mg (52% based on ligand 3-Htba) of product. IR (KBr; cm^{-1}): 3431 (br, m), 3128(m), 3088(m), 1643(s), 1625(s), 1582(s), 1532(m), 1386(s), 1365(s), 1265(w), 1231(w), 1090(m), 1046(m), 903(w), 875(w), 771(m), 734(m), 688(w), 663(w), 556(w).

Synthesis of [Zn(3-tba)$_2$] (1β). As-synthesized **1α** was heated at 150 °C under vacuum for 12 h to afford **1β**. IR (KBr; cm^{-1}): 3426(br, m), 3109(w), 3069(s), 1625(m), 1582(s), 1535(s), 1387(s), 1366(s), 1265(w), 1235(w), 1090(m), 1042(m), 871(w), 771(m), 733(m), 690(w), 666(w), 549(w). The single crystals of **1β** was obtained by exchanging the solvent in the as-synthesized **1α** with anhydrous CH_2Cl_2 for 5 days, followed by evacuation under a dynamic vacuum at room temperature overnight.

Synthesis of [Zn(3-tba)$_2$]·2H$_2$O (2). An open 10 mL vial containing **1β** was placed in a sealed 25 mL vial containing 4 mL water for 24 h to afford **2**, and the single crystals of **2** was also obtained by this method. IR (KBr; cm^{-1}): 3419(br, m), 3144(w), 2831(w), 1600(s), 1390(m), 1367(s), 1090(m), 1264(w), 1230(w), 1090(m), 1046(m), 903(w), 875(w), 770(m), 733(m), 687(w), 662(w), 555(w).

2. Single-crystal X-ray diffraction measurements

Diffraction intensities of the compounds **1α**, **1β** and **2** was collected at room temperature on a Bruker Apex CCD diffractometer with graphite-monochromated Mo K_α (λ = 0.71073 Å, for **1α**) or Cu K_α (λ = 1.54178 Å, for **1β** and **2**) radiation. In all cases, data was indexed, integrated and scaled in APEX3.[2] Absorption correction was performed by multi-scan method using in SADABS.[3] Space group was determined using XPREP[4] implemented in APEX3. Structures were solved using intrinsic phasing method (SHELXT)[5] and refined on F^2 using nonlinear least-squares techniques with SHELXL programs.[6] Anisotropic thermal parameters were

applied to all non-hydrogen atoms. The hydrogen atoms of the water molecules were located in a difference Fourier map, and the other hydrogen atoms were generated geometrically. Crystal data and structure refinement are summarized in Table S1. Crystallographic data of **1**α, **1**β and **2** has been deposited in the Cambridge Crystallographic Data Center with reference numbers 2160142-2160144.

3. Single-crystal data and structural parameters

Table S1. Crystallographic data and structure refinement summary for **1**α, **1**β and **2**.

Compounds	**1**α	**1**β	**2**
Formula	$C_{22}H_{21}N_7O_5Zn$	$C_{18}H_{12}N_6O_4Zn$	$C_{18}H_{16}N_6O_6Zn$
Formula weight	528.83	441.71	477.74
Crystal system	Triclinic	Triclinic	Triclinic
Space group	*P*-1	*P*-1	*P*-1
α (Å)	6.9713(8)	6.5102(9)	6.3098(10)
b (Å)	12.0179(7)	7.7166(12)	7.1905(12)
c (Å)	14.2464(8)	17.682(3) Å	20.346(3)
α (deg)	72.986(3)	102.090(9)	98.586(9)
β (deg)	87.232(4)	91.927(12)	94.474(8)
γ (deg)	83.640(4)	100.163(9)	91.396(9)
V (Å^3)	1134.15(2)	852.6(2)	909.4(3)
Z	2	2	2
D_c (g·cm^{-3})	1.549	1.720	1.745
μ (mm^{-1})	1.133	2.386	2.371
R_{int}	0.0393	0.0993	0.0748
GOF	1.059	1.019	1.028
R_1 [$I > 2\sigma(I)$]	0.0564	0.1173	0.1156
wR_2 [all data]	0.1490	0.3149	0.2862
Diff peak, hole (e Å^{-3})	1.803, -0.783	0.970, -0.599	0.958, -0.503
CCDC number	2160142	2160143	2160144

$R_1 = \sum||F_o| - |F_c||/\sum|F_o|$. $wR_2 = [\sum w(F_o^2 - F_c^2)^2/\sum w(F_o^2)^2]^{1/2}$

4. Additional structure figures

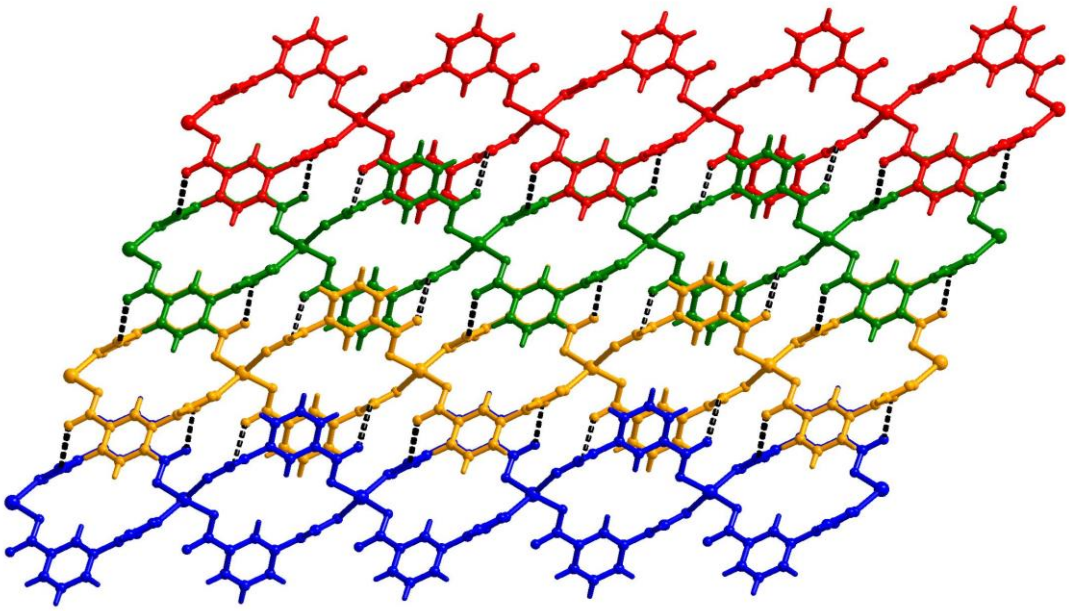

Figure S1. The C-H···O weak interactions among 1D chains in **1*α***.

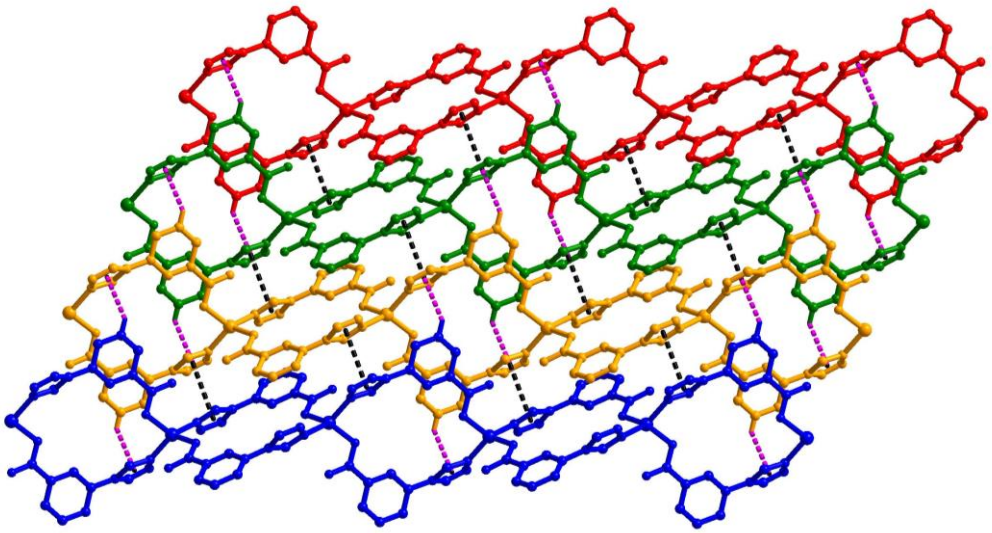

Figure S2. The π···π stacking interactions between the triazole rings (showing in black dash line; *d* (Cg···Cg) = 3.510 Å; interplanar distance = 3.489(2)-3.494(2) Å) and C-H···π interactions (showing in purple dash line; *d* (H···Cg) = 2.90 Å ; *d* (X···Cg) = 3.520(5) Å; ∠(C-H···Cg = 126°) between adjacent 1D chains in **1*α***.

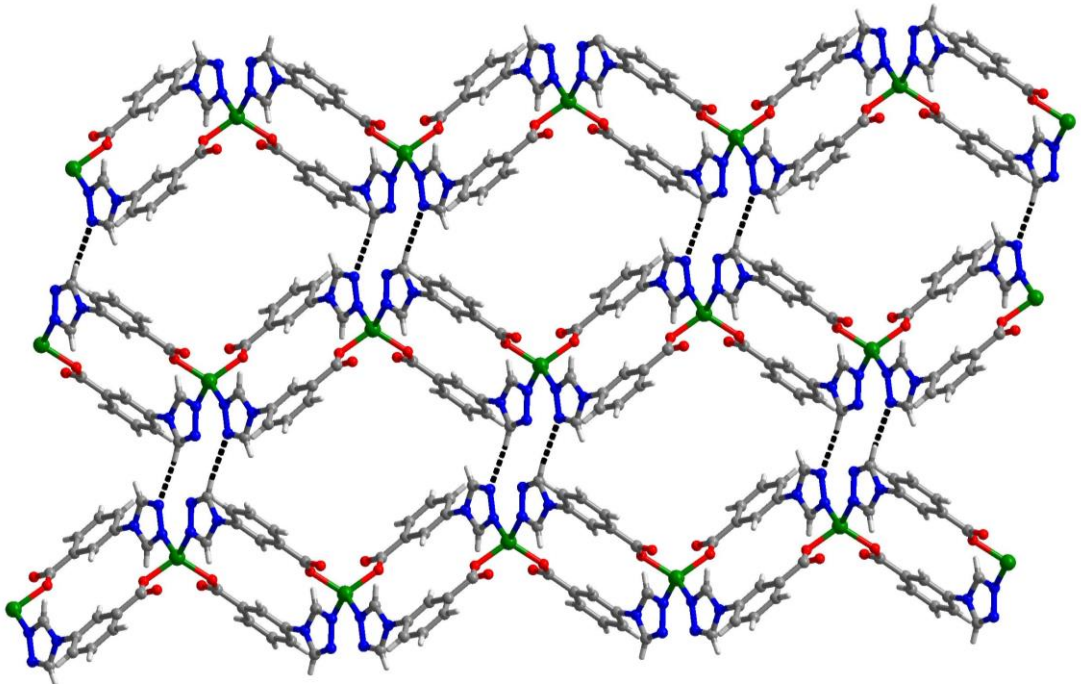

Figure S3. The C-H···N stacking weak interactions among adjacent 1D chains along crystallographic *a*-axis in **1*α***.

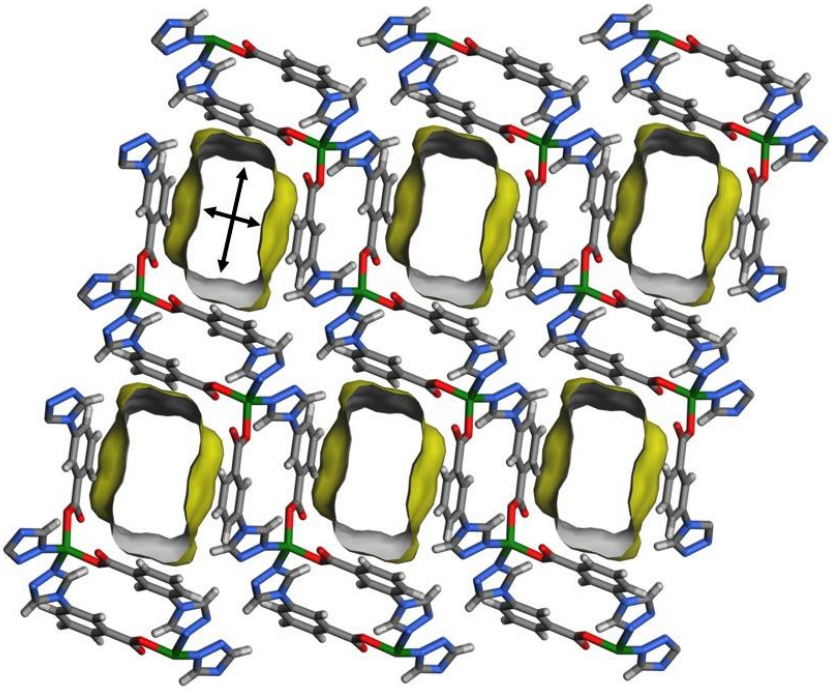

Figure S4. Illustrations of 3D stacking structure and the position of pore diameters (approximately 4.9 × 7.3 Å^2) viewed along the *a*-axis for **1*α***.

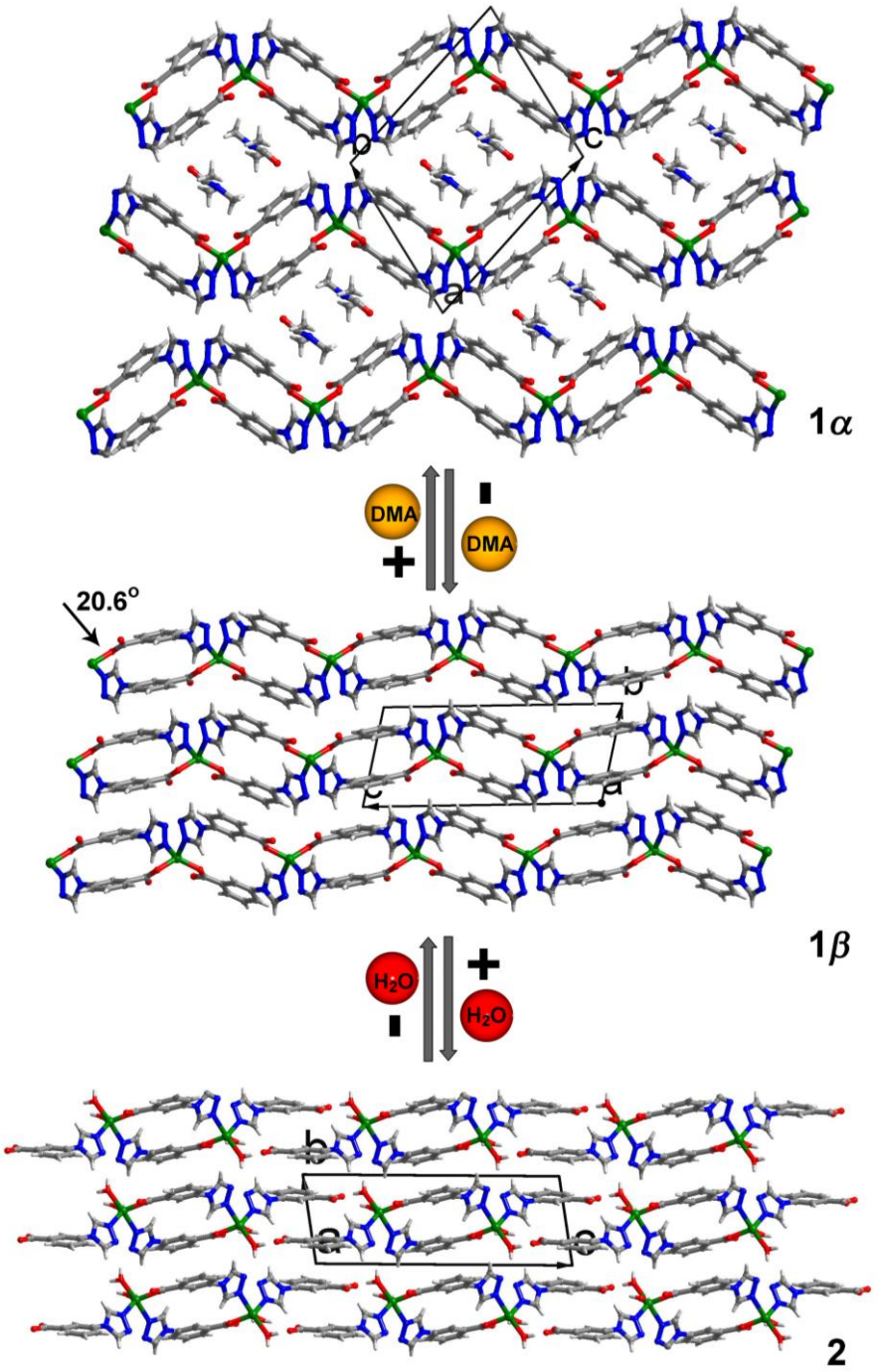

Figure S5. The packing diagram viewed along *a*-axis showing the structural transformations among **1**α, **1**β and **2** (the arrow point out the deviation angle of one Zn-carboxylate bond with the carboxylate group plane in **1**β).

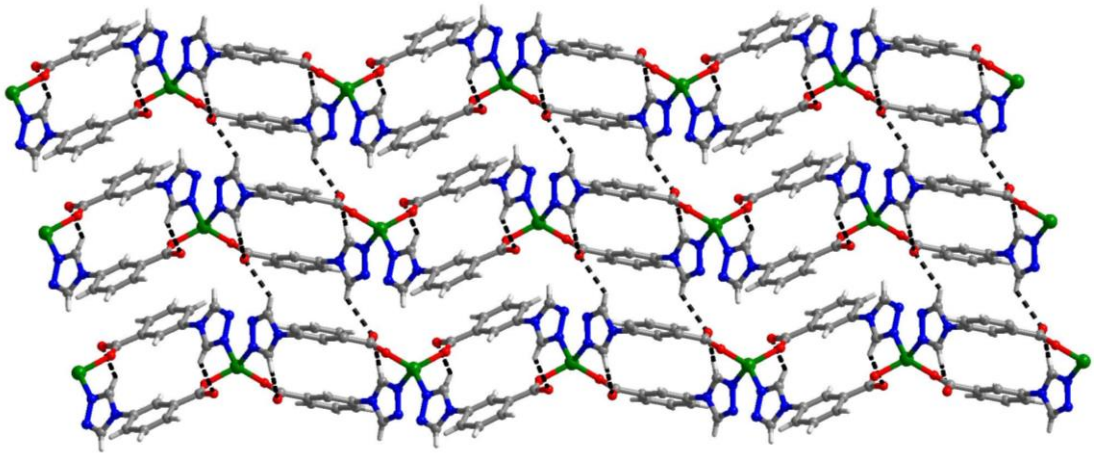

Figure S6. The C-H···O weak interactions among 1D chains viewed along crystallographic *a*-axis in **1***β*.

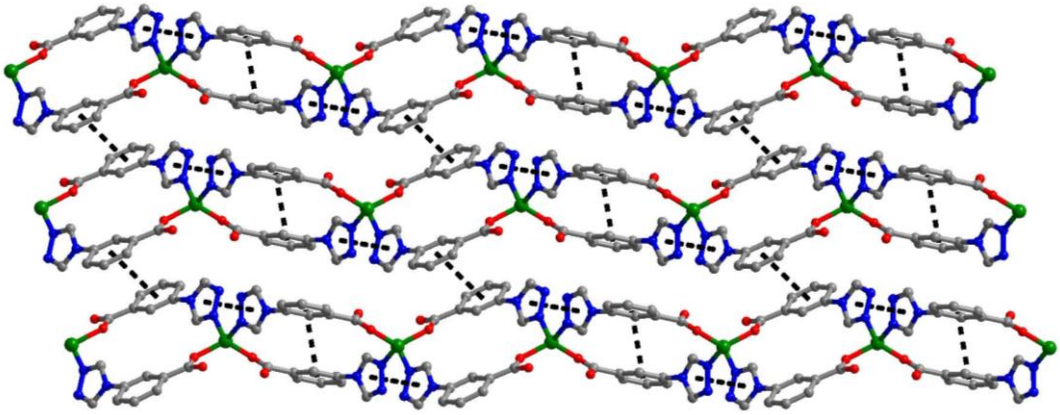

Figure S7. The π···π stacking interactions in **1***β*.

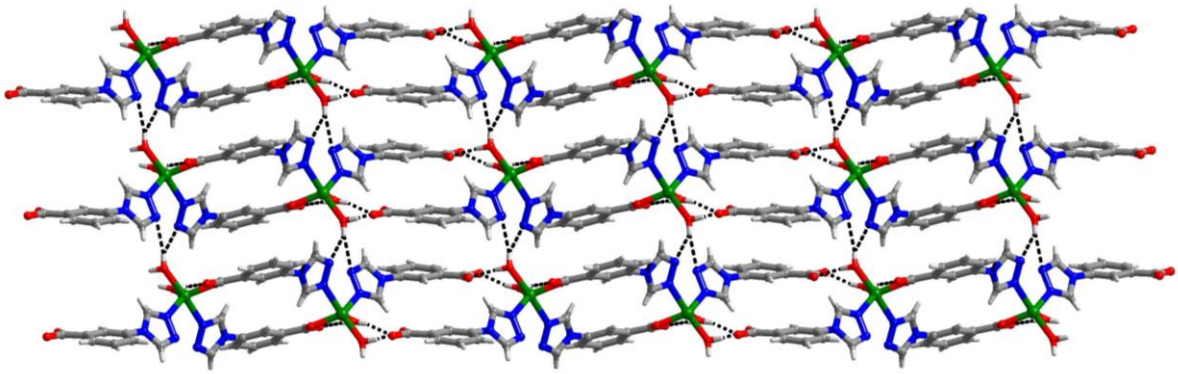

Figure S8. The O-H···O and O-H···N hydrogen bonds viewed along crystallographic *a*-axis in **2**.

5. Summary tables of structural differences among 1α, 1β and 2.

Table S2. Comparative analysis of structural differences among **1α, 1β and 2.**

Compounds	**1α**	**1β**	**2**
Coordination geometry of Zn^{2+} ions	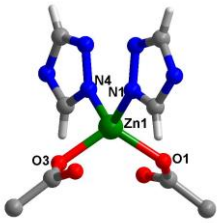 Zn-O: 1.955(3)/1.960(3) Å Zn-N: 2.025(3)/2.031(3) Å ∠O-Zn-O: 112.05(14)° ∠O-Zn-N: 94.72(13)°-123.50(14)° ∠N-Zn-N: 110.87(13)°	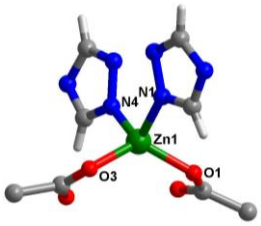 Zn-O: 1.924(9)-1.991(9) Å Zn-N: 2.025(10)-2.058(10) Å ∠O-Zn-O: 118.8(4)° ∠O-Zn-N: 94.5(4)°-123.4(4)° ∠N-Zn-N: 107.0(4)	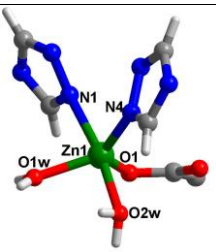 Zn-O: 1.988(9) -2.102(9) Zn-N: 2.035(10)-2.251(10) Å ∠O-Zn-O: 86.7(4)°-112.3(4)° ∠O-Zn-N: 84.6(4)°-170.9(4)° ∠N-Zn-N: 92.9(4)°
Geometry parameters between the zinc ion and carboxylate plane	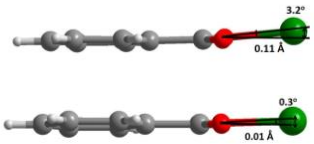	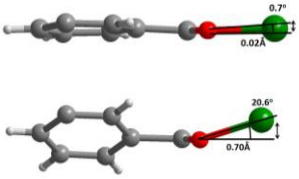	
dihedral angles of between triazole and benzene rings)	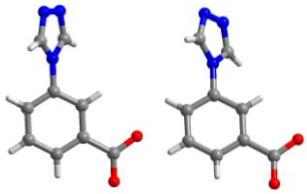 53.0° / 130.2°	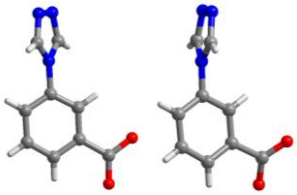 76.9° / 134.4°	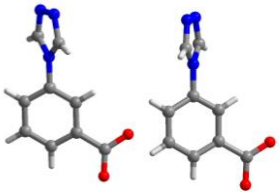 126.4° / 128.0°
The nearby Zn···Zn distance in the $[Zn_2(3\text{-tba})_2]$ ring	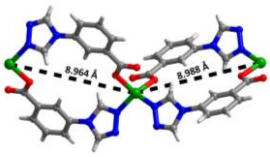	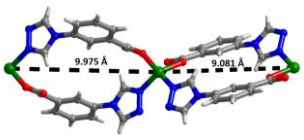	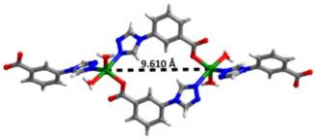

6. Summary tables of weak interactions in the 1α, 1β and 2.

Table S3. Possible hydrogen bonds in **1α**, **1β** and **2**.

	D-H	H···A	D···A	∠D-H···A
1α				
C(1)-H(1A)···O(2a)	0.93	2.44	3.097(6)	128
C(10)-H(10A)···O(4b)	0.93	2.39	3.049(6)	127
C(11)-H(11A)···N (2c)	0.93	2.57	3.486(6)	168
1β				
C(1)-H(1A)···O(2c)	0.93	2.58	3.213(18)	126
C(10)-H(10A)···O(4d)	0.93	2.36	2.912(17)	117
C(11)-H(11A)···O(4e)	0.93	2.50	3.159(16)	128
2				
O(1W)-H(1WA)···O(4b)	0.85	1.71	2.535(14)	164
O(1W)-H(1WB)···O(2f)	0.85	1.89	2.737(14)	179
O(2W)-H(2WA)···N(5g)	0.85	2.58	3.254(15)	137
O(2W)-H(2WA)···N(2h)	0.85	2.43	3.146(14)	143
O(2W)-H(2WB)···O(3b)	0.85	1.78	2.626(13)	171
C(10)-H(10A)···O(4i)	0.93	2.58	3.155(16)	121
C(11)-H(11A)···O(4j)	0.93	2.35	3.241(17)	161

Note: the weak hydrogen bonds exclude the interactions between the uncoordinated solvent molecules and 1D chains). Symmetry code: (a) –x+2, -y, -z+1; (b) –x+1, -y+1, -z; (c) –x+1, -y+1, -z+1; (d) –x+1, -y+1, -z+2; (e) –x+1, -y, -z+2; (f) x+1, y, z; (g) x, y+1, z; (h) –x+2, -y+2, -z+1; (i) –x, -y+1, -z; (j) –x, -y, -z.

Table S4. Analysis of shortest aromatic π-π stacking interaction in **1α**, **1β** and **2**.

	distance between ring centroids	distance between ring centroid to plane	distance between ring centroid to plane
1α			
triazole-triazole	3.510(2)	3.489(2)	3.494(2)
1β			
triazole- triazole	3.416(7)	3.388(5)	3.403(5)
benzene-benzene	3.784(8)	3.549(6)	3.549(6)
benzene-benzene	3.725(8)	3.535(5)	3.535(5)
2			
benzene-benzene	3.490(8)	3.290(5)	3.291(5)
benzene-benzene	3.574(8)	3.435(5)	3.435(5)

Table S5. Possible C-H···π interactions in **1α**, **1β** and **2**.

	H···Cg	X···Cg	∠X-H···Cg
1α			
C (16)-H(16A)···Cg	2.90	3.520(5)	126
1β			
C(7)-H(7A)···Cg	2.98	3.441(15)	112
2			
C(7)-H(7A)···Cg	2.79	3.394(14)	123

7. Powder X-ray diffraction (PXRD)

Powder X-ray diffraction (PXRD) patterns were recorded at the room temperature on a Rigaku MiniFlex600 X-ray diffractometer (40 KV, 15 mA) with Cu-Kα (λ = 1.5405 Å) radiation in a 2theta range from 3 to 50°. All the calculated PXRD patterns are simulated from single-crystal diffraction by using Mercury v3.8 software (Cambridge Crystallographic Data Centre, Cambridge, UK)

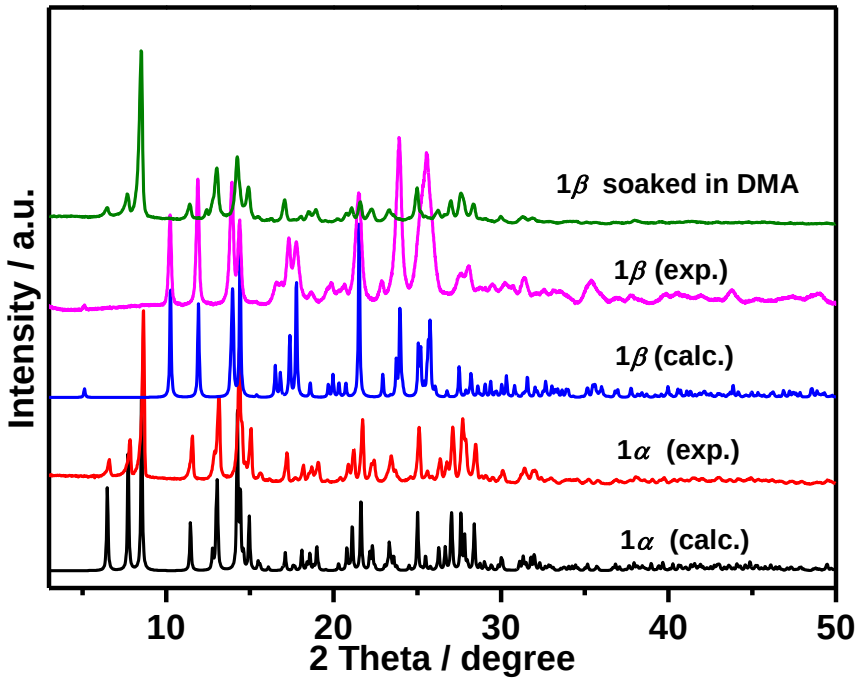

Figure S9. PXRD patterns of **1**α, **1**β, and **1**β after soaking in DMF for 24 h.

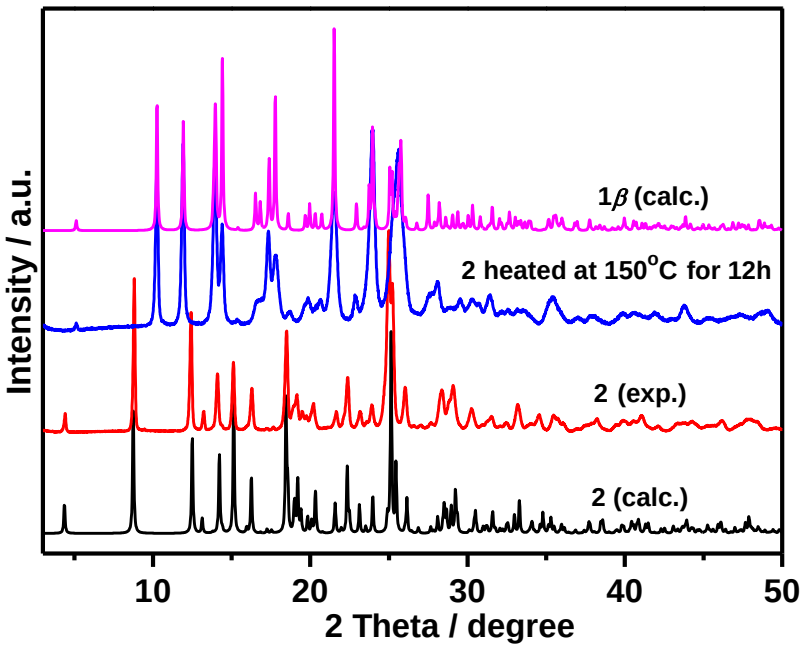

Figure S10. PXRD patterns of **2** and **2** after heating at 150°C for 12 h.

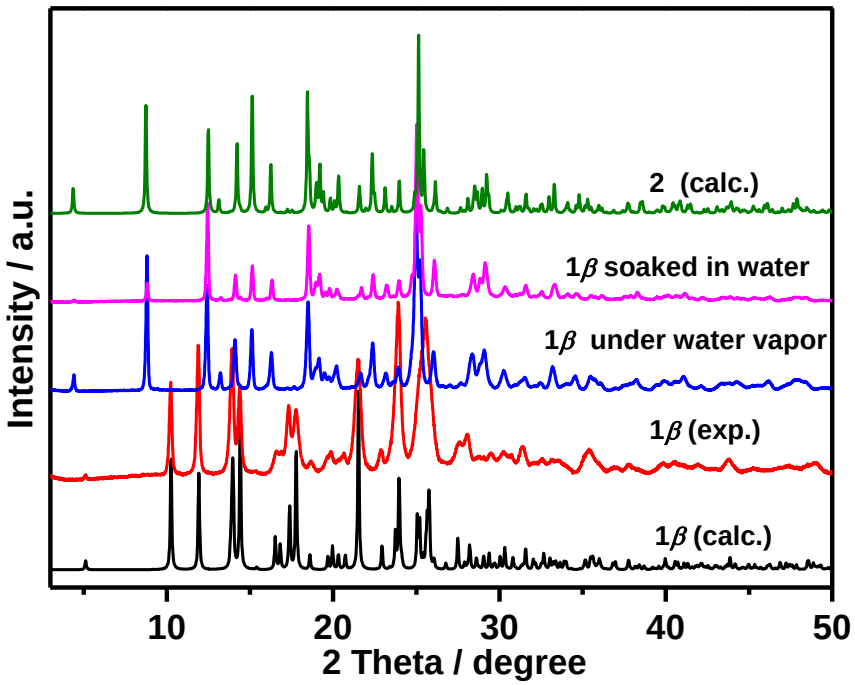

Figure S11. PXRD patterns of **1*β***, **1*β*** under water vapour (vial-in-vial method) for 24 h, **1*β*** after soaking in water for one day and **2**.

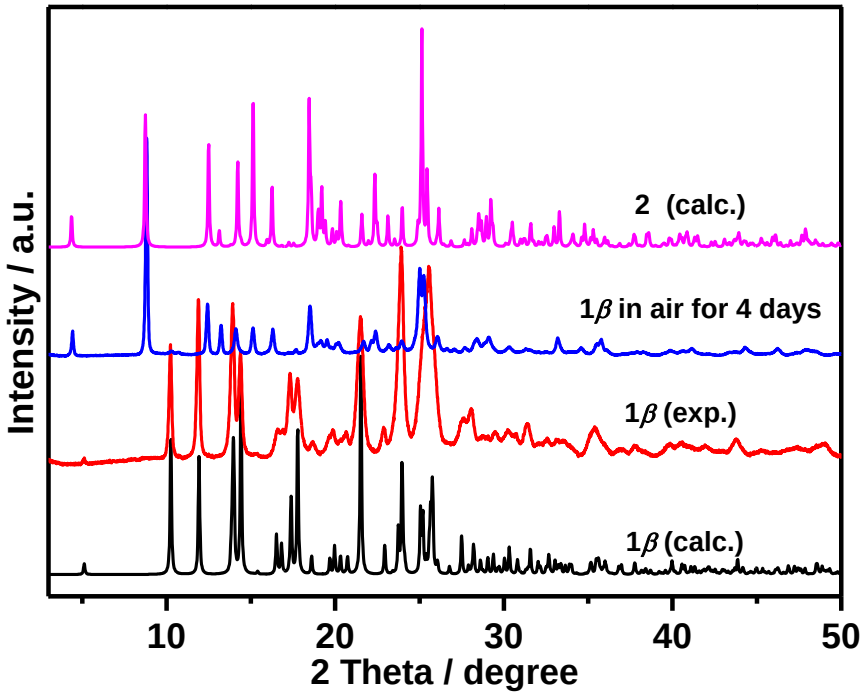

Figure S12. PXRD patterns of **1**β, **2** and **1**β exposed to humid air (*ca*. 45% RH).

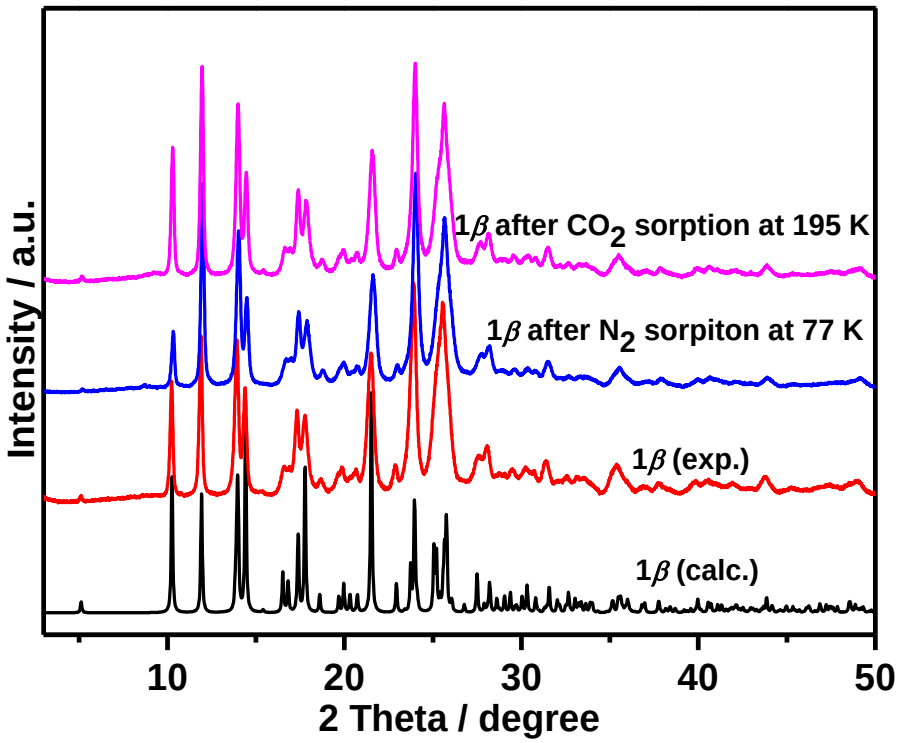

Figure S13. PXRD patterns of **1**β after N_2 (77 K) and CO_2 (195 K) sorption.

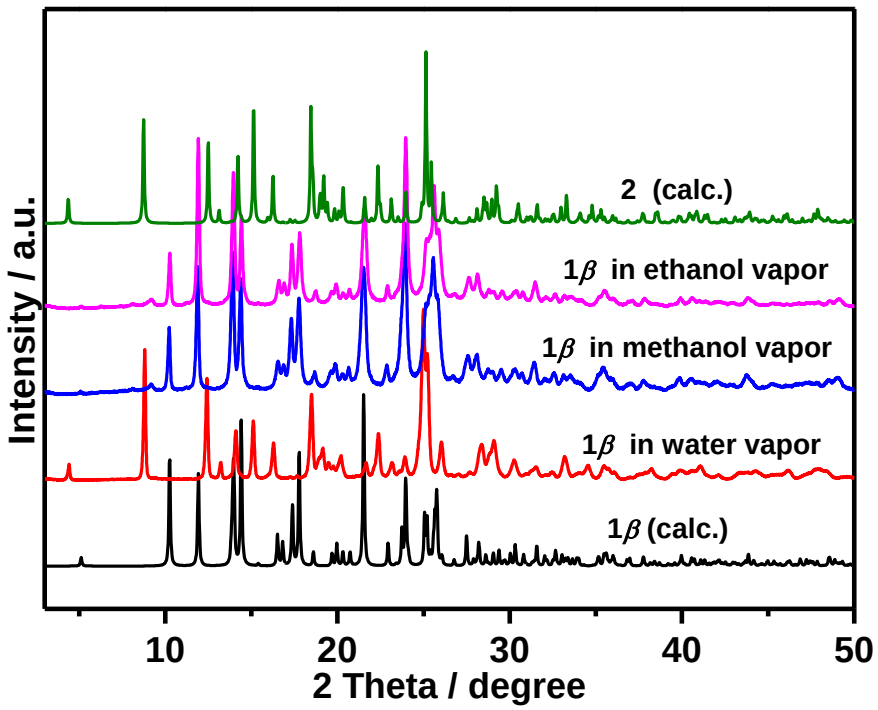

Figure S14. PXRD patterns of **1*β*** exposed under different vapor conditions (vial-in-vial method: an open 10 mL vial containing 30 mg of **1*β*** adsorbent was placed in sealed 25 mL vial containing 4 mL water, ethanol and methanol pure solvent) for 24 h. Obviously, only water vapor can make **1*β*** convert to **2**.

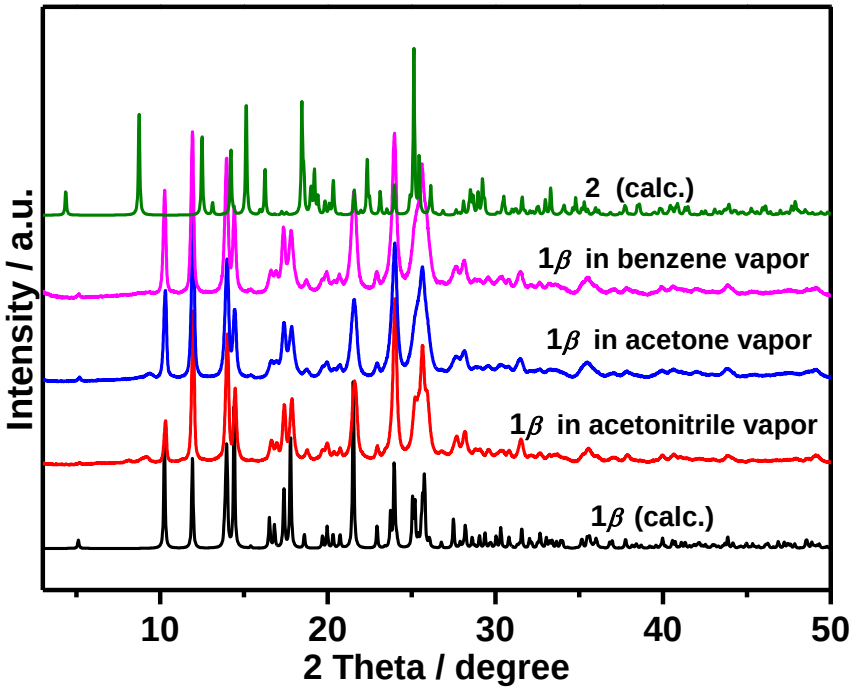

Figure S15. PXRD patterns of **1*β*** exposed under different vapor conditions (vial-in-vial method: an open 10 mL vial containing 30 mg of **1*β*** adsorbent was placed in sealed 25 mL vial containing 4 mL acetonitrile, acetone and benzene pure solvent) for 24 h. **1*β*** can keep the same structure, and can't convert to **2** under acetonitrile, acetone and benzene vapor conditions.

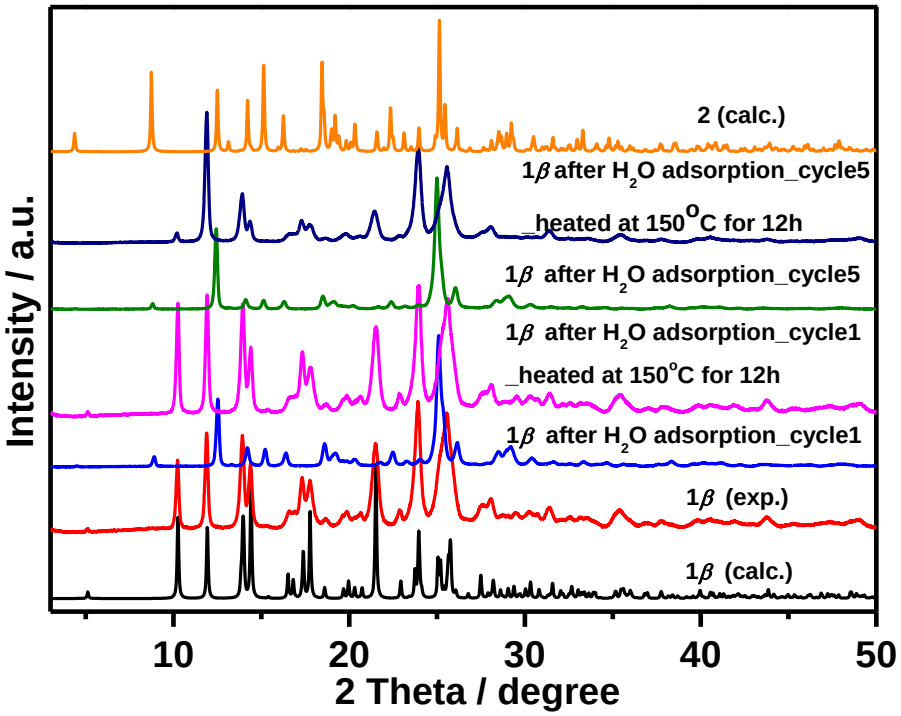

Figure S16. PXRD patterns of **1*β*** under different conditions. After the first cycle of water sorption/desorption, **1*β*** had converted to **2**. When heating the **2** (converted from **1*β***) at 150 °C under vacuum for 12 h, it had once again converted to **1*β***. The sample converted to **2** again when we perform the fifth cycle of water absorpiton /desorpiton at room temperature, and then converted back to **1*β*** again when heating at 150 °C under vacuum for 12 h.

8. Thermogravimetric analysis (TGA)

Thermogravimetric analysis (TGA) performed using a Netzsch STA 449C instrument with a heating rate of 10.0 °C/min from the room temperature to 600 °C under N_2 atmosphere.

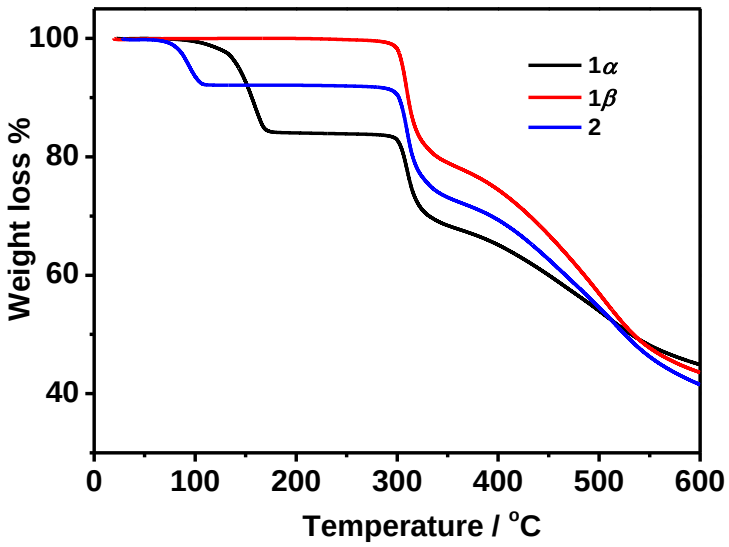

Figure S17. TG curves of **1**α, **1**β and **2** in a N_2 environment. The TGA urve of **1**α displays a weight loss of 16.42% at 290 °C, resulting from the release of one molecules of DMA per formula unit (calc. 16.47%). The TG curves of **2** show no weight loss, indicating that there is no guest in **1**β. The TGA curve of **2** displays a weight loss of 7.89% at 175 °C, resulting from the release of two molecules of water per formula unit (calc. 7.54%).

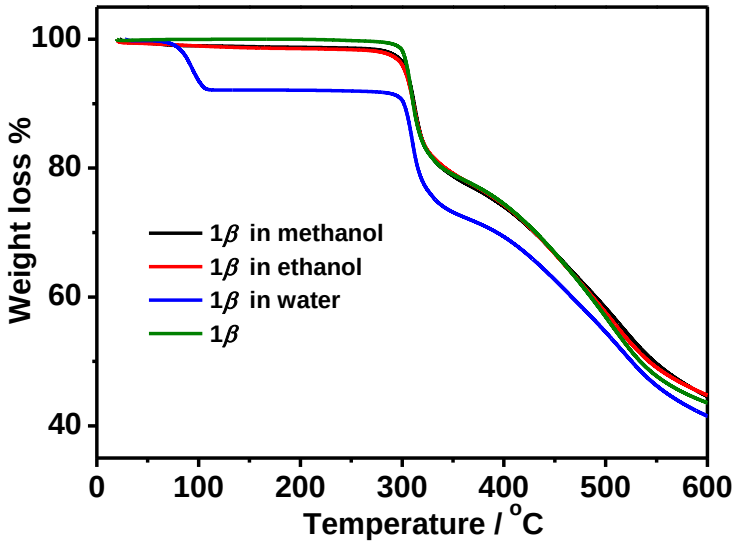

Figure S18. TG curves of **1**β after exposure to the vapors of water, methanol and ethanol for 24 h (vial-in-vial method: an open 10 mL vial containing 30 mg of **1**β was placed in sealed 25 mL vial containing 4 mL water, ethanol and methanol pure solvent, respectively) before performing TG experiments. The sample of **1**β exposed to methanol and ethanol show almost no weight loss. However, **1**β show obviously weight loss after exposure to water vapour, the weight loss of 7.89% at 175 °C, corresponding to the release of two water molecules per formula unit (calc. 7.54%)

9. IR spectra

Infrared spectra were recorded from KBr pellets on a Thermo Scientific Nicolet IS 10 FTIR spectrometer in the range of 400-4000 cm^{-1}.

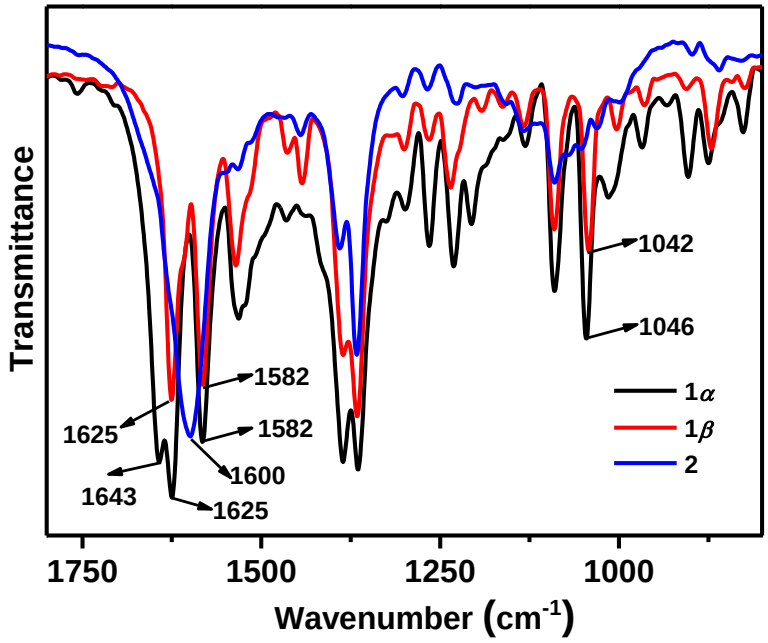

Figure S19. IR spectra of **1*α***, **1*β*** and **2**. The lack of C=O stretching peaks at about 1643 cm^{-1} in the IR spectra of **1*β*** confirms the full release of DMA guests. In contrast to **1*α*** and **1*β***, IR spectrum of **2** indicates an appearance of a new peak at 1600 cm^{-1} and disappearance of two peaks at 1625 and 1582 cm^{-1}, and meanwhile, the intensity of peaks at 1042-1046 cm^{-1} were greatly induced. IR analyses reveal that the cleavage of coordination bond on carboxylate groups and formation of new coordination bond in **2**.

10. Gas and vapor adsorption

The gas adsorption isotherms for N_2 and CO_2 were performed at 77 K and 195 K, respectively. The vapor adsorption for water, methanol, ethanol, acetonitrile, acetone and benzene measured at room temperature (298 K). All the adsorption isotherms were measured by using Belsorp-max gas adsorption instrument (MicrotracBEL Corp from Japan), respectively. Before gas sorption experiment, the samples of **1*β*** was activated under high vacuum at 150 °C for 12 h to remove the remnant solvent molecules prior to measurements.

For other consecutive cycles of water adsorption, the same batch of samples was activated at 150 °C under high vacuum degased for 12 h before gas sorption experiments.

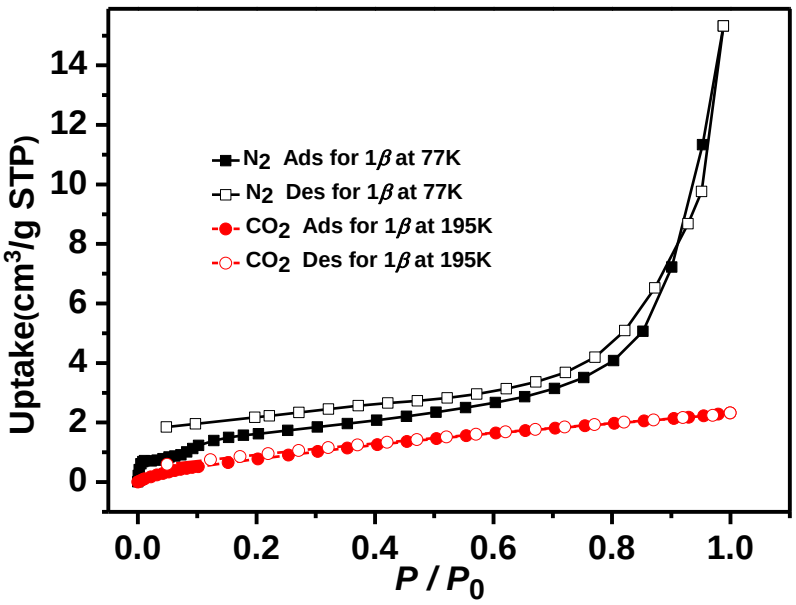

Figure S20. Gas sorption isotherms of **1*β*** at 77 K (N_2) and at 195 K (CO_2).

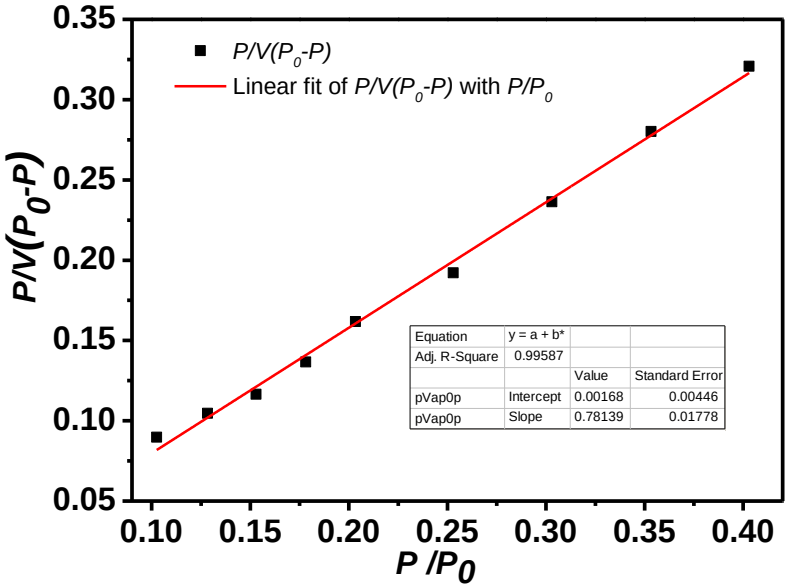

Figure S21. BET plot for the N_2 adsorption isotherm of **1*β*** at 77 K, and the range P/P_0 from 0.1026 to 0.403 satisfies for applying the BET theory.

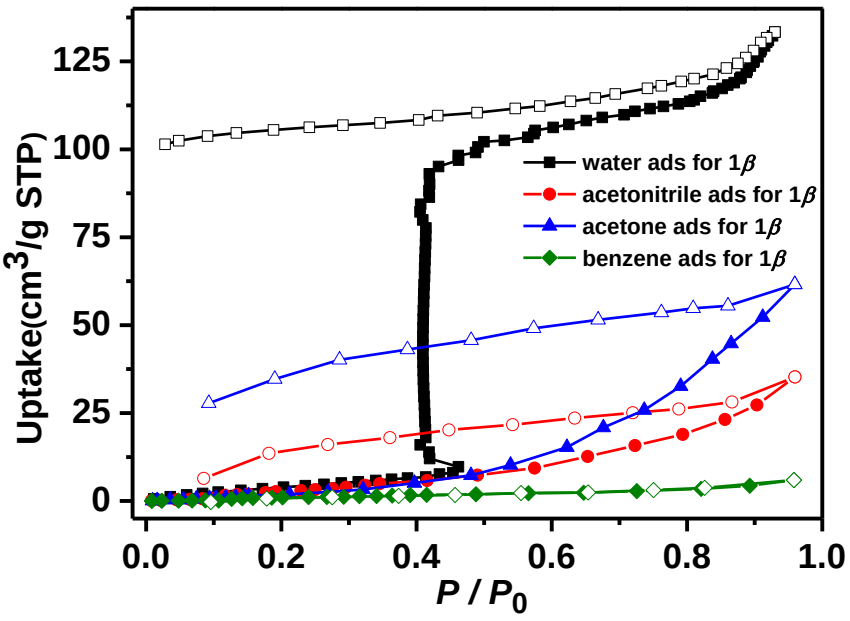

Figure S22. Water, acetonitrile, acetone and benzene vapor sorption isotherms of **1*β*** at 298 K.

11. Summary of MOMs with type F-IV water adsorption isotherms

Table S6. Summary of MOMs with type F-IV water adsorption isotherms.

Sorbents	Dimension	water adsorption mechanism	Adsorption isotherm	Saturation uptake (cm^3/g)	P_{ga}	Ref.
[Zn(3-tba)$_2$] (1*β*)	1D	1D→0D changes	F-IV^S	118 (298 K)	P/P_0 = 0.46	This work
[Cu(PF$_6$)$_2$(bpetha)$_2$]$_n$	1D	1D→1D changes	F-IV^S	112 (298 K)	P/P_0 = 0.80	[7]
[Cu(PF$_6$)$_2$(bpetha)(2,2'-bpy)]$_n$	1D	1D→1D changes	F-IV^S	58 (298 K)	P/P_0 = 0.07	
[Co(Hdpd)$_2$(bpy)]$_n$	1D	/	F-IV^S	110 (298 K)	$P/P_0 \approx 0.63$	[8]
[Ni(Hdpd)$_2$(bpy)]$_n$	1D	/	F-IV^S	109 (298 K)	$P/P_0 \approx 0.49$	
[Zn(H$_2$SSA)$_2$(H$_2$O)$_2$]	1D	1D→0D changes	F-IV^m	500 (298 K)	$P/P_0 \approx 0.30$ $P/P_0 \approx 0.33$	[9]
CID-5	2D	/	F-IV^S	260 (298 K)	$P/P_0 \approx 0.78$	[10]
CuCID-1	2D	2D→2D changes	F-IV^S	174 (298 K)	P/P_0 = 0.33	[11]
ZnCID-1	2D	2D→2D changes	F-IV^S	162 (298 K)	P/P_0 = 0.60	
Mn[Ni(CN)$_4$]	amorphous	amorphous→2D	F-IV^S	669 (298 K)	P/P_0 = 0.40	[12]
Fe[Ni(CN)$_4$]	amorphous	amorphous→2D	F-IV^S	656 (298 K)	P/P_0 = 0.60	
Co[Ni(CN)$_4$]	amorphous	amorphous→2D	F-IV^S	647 (298 K)	P/P_0 = 0.90	
[Mn(NNdmenH)][Cr(CN)$_6$]	3D	3D→2D changes	F-IV^m	146 (298 K)	$P/P_0 \approx 0.034$ P/P_0 = 0.08	[13]
[Ce(tci)]$_n$	3D	3D→2D changes	F-IV^S	186 (298 K)	$P/P_0 \approx 0.12$	[14]
[[Cu$_2$(pzdc)$_2$(dpyg)]$_n$	3D	3D→3D changes	F-IV^S	/	/	[15]
DUT-98(3)	3D	3D→3D changes	F-IV^S	627 (298 K)	P/P_0 = 0.50	[16]
MAF-7	3D	pore filling	F-IV^S	551 (298 K)	$P/P_0 \approx 0.23$	[17]
MIL-101-NH$_2$	3D	pore filling	F-IV^m	1157 (298 K)	$P/P_0 \approx 0.37$ $P/P_0 \approx 0.42$	[18]
MIL-101-NO$_2$	3D	pore filling	F-IV^m	498 (298 K)	$P/P_0 \approx 0.40$ $P/P_0 \approx 0.50$	
CAU-10-H	3D	pore filling	F-IV^S	382 (298 K)	$P/P_0 \approx 0.18$	[19a]
				358 (298 K)	$P/P_0 \approx 0.17$	[19b]
				448 (298 K)	$P/P_0 \approx 0.11$	[19c]
CAU-10-OCH$_3$	3D	pore filling	F-IV^S	92 (298 K)	$P/P_0 \approx 0.25$	[19a]
In-MIL-68	3D	pore filling	F-IV^S	398 (298 K)	$P/P_0 \approx 0.56$	[20]

In-MIL-68-NH_2	3D	pore filling	F-IV^S	423 (298 K)	$P/P_0 \approx 0.42$	
MOF-841	3D	pore filling	F-IV^S	640 (298 K)	$P/P_0 = 0.20$	[21]
PIZOF-2	3D	pore filling	F-IV^S	850 (298 K)	$P/P_0 = 0.70$	
UiO-67	3D	pore filling	F-IV^S	365 (298 K)	$P/P_0 \approx 0.52$	[22]
CAU-1	3D	pore filling	F-IV^S	437 (298 K)	$P/P_0 \approx 0.33$	[19b]
NOTT-400	3D	pore filling	F-IV^S	560 (303 K)	$P/P_0 \approx 0.25$	[23]
UIO-67-BN	3D	pore filling	F-IV^S	614 (303 K)	$P/P_0 = 0.53$	[24]
Y-shp-MOF-5	3D	pore filling	F-IV^S	548 (298 K)	$P/P_0 \approx 0.50$	[25]
UiO-66	3D	pore filling	F-IV^m	495 (298 K)	$P/P_0 = 0.25$ $P/P_0 = 0.40$	[26a]
			F-IV^S	684 (298 K)	$P/P_0 = 0.25$	[26b]
Al-fumarate	3D	pore filling	F-IV^S	597 (298 K)	$P/P_0 = 0.20$	[27a]
				525(303 K)	$P/P_0 \approx 0.20$	[27b]
				560 (298 K)	$P/P_0 \approx 0.20$	[19c]
Cr-soc-MOF-1	3D	pore filling	F-IV^S	2428 (298 K)	$P/P_0 \approx 0.55$	[28]
BUT-46A	3D	pore filling	F-IV^S	645 (298 K)	$P/P_0 = 0.44$	[29]
BUT-46B	3D	pore filling	F-IV^S	614 (298 K)	$P/P_0 = 0.51$	
BUT-46F	3D	pore filling	F-IV^S	735 (298 K)	$P/P_0 = 0.39$	
ZIF-90	3D	pore filling	F-IV^S	421 (298 K)	$P/P_0 \approx 0.30$	[30a]
			F-IV^S	392 (298 K)	$P/P_0 \approx 0.30$	[30b]
MIL-101	3D	pore filling	F-IV^m	1742 (298 K)	$P/P_0 = 0.40$ $P/P_0 = 0.44$	[31a]
			F-IV^m	1792 (298 K)	$P/P_0 \approx 0.28$ $P/P_0 \approx 0.30$	[31b]
			F-IV^s	1319 (298 K)	$P/P_0 \approx 0.38$	[31c]
NU-1500-Cr	3D	pore filling	F-IV^S	1360 (298 K)	$P/P_0 \approx 0.45$	[32]
Co-CUK-1	3D	pore filling	F-IV^S	373 (303 K)	$P/P_0 \approx 0.12$	[33]
Ni-CUK-1	3D	pore filling	F-IV^S	398 (303 K)	$P/P_0 = 0.12$	
Mg-CUK-1	3D	pore filling	F-IV^S	448 (303 K)	$P/P_0 = 0.25$	
DMOF-TM	3D	pore filling	F-IV^S	515 (298 K)	$P/P_0 \approx 0.25$	[34]
Al-MIL-53	3D	pore filling	F-IV^S	460 (298 K)	$P/P_0 \approx 0.54$	[35a]
				548 (298K)	$P/P_0 \approx 0.38$	[35b]
MIL-53-TDC	3D	pore filling	F-IV^S	473 (293 K)	$P/P_0 \approx 0.25$	[36]
Fe-MIL-101-propyonylamido	3D	pore filling	F-IV^m	840 (298 K)	$P/P_0 \approx 0.38$ $P/P_0 \approx 0.52$	[37]
Fe-MIL-101-butyrylamido	3D	pore filling	F-IV^m	721 (298 K)	$P/P_0 \approx 0.38$ $P/P_0 \approx 0.53$	
Fe-MIL-101-naphthoylamido	3D	pore filling	F-IV^m	616 (298 K)	$P/P_0 \approx 0.30$ $P/P_0 \approx 0.42$	
Fe-MIL-101-cyclohexanoylamido	3D	pore filling	F-IV^S	542 (298 K)	$P/P_0 \approx 0.34$	
Fe-MIL-101-phenylamido	3D	pore filling	F-IV^m	428 (298 K)	$P/P_0 \approx 0.35$ $P/P_0 \approx 0.51$	
MIL-160	3D	pore filling	F-IV^S	423 (323 K)	$P/P_0 \approx 0.07$	[38]
EHU-30(Zr)	3D	pore filling	F-IV^S	539 (298 K)	$P/P_0 = 0.35$	[39]
NU-913	3D	pore filling	F-IV^S	1149 (298K)	$P/P_0 \approx 0.50$	[40]
MOF-808-Formate	3D	pore filling	F-IV^S	840 (298K)	$P/P_0 \approx 0.28$	[41]

F-IV^s: single-step type F-IV; F-IV^m: multiple-step (≥2) F-IV; P_{ga}: the pressure of gate-opening.

References

1. T. Panda, P. Pachfule and R. Banerjee, *Chem. Commun.*, 2011, **47**, 7674-7676.
2. APEX3. Ver. 2017.3-0. Bruker AXS Inc., Madison, Wisconsin, USA, 2017.
3. L. Krause, R. Herbst-Irmer, G. M. Sheldrick and D. Stalke, *J. Appl. Cryst.*, 2015, **48**, 3-10.
4. XPREP Ver. 2014/2, Bruker AXS Inc., Madison, Wisconsin, U SA, 2014.
5. G. Sheldrick, *Acta Cryst. A*, 2015, **71**, 3-8.
6. G. Sheldrick, *Acta Cryst. C*, 2015, **71**, 3-8.
7. S. I. Noro, K. Fukuhara, K. Kubo and T. Nakamura, *Cryst. Growth Des.*, 2011, **11**, 2379-2385.
8. X.-Y. Cao, L. Li, C.-X. Li, L. Lv and R.-D. Huang, *CrystEngComm*, 2015, **17**, 2398-2405.
9. J. H. Song, D. W. Kim, D. W. Kang, W. R. Lee and C. S. Hong, *Chem. Commun*., 2019, **55**, 9713-9716.
10. T. Fukushima, S. Horike, Y. Inubushi, K. Nakagawa, Y. Kubota, M. Takata and S. Kitagawa, *Angew Chem., Int Ed.*, 2010, **49**: 4820-4824.
11. Y. Kamakura, A. Hikawa, H. Yoshikawa, W. Kosaka, H. Miyasaka and D. Tanaka, *Chem Commun.*, 2020, **56**: 9106-9109.
12. H. Yoshino, K. Yamagami, H. Wadati, H. Yamagishi, H. Setoyama, S. Shimoda, A. Mishima, B. Le Ouay, R. Ohtani and M. Ohba, *Inorg Chem.*, 2021, **60**, 3338-3344.
13. W. Kaneko, M. Ohba and S. Kitagawa, *J. Am. Chem. Soc.*, 2007, **129**, 13706-13712.
14. S. K. Ghosh, J.-P. Zhang and S. Kitagawa, *Angew Chem., Int Ed.*, 2007, **46**, 7965-7968.
15. R. Kitaura, K. Fujimoto, S. -I. Noro, M. Kondo and S. Kitagawa, *Angew. Chem., Int. Ed.*, 2002, **41**, 133-135.
16. S. Krause, V. Bon, H. Du, R. E. Dunin-Borkowski, U. Stoeck, I. Senkovska and S. Kaskel, *Beilstein J Nanotechnol.*, 2019, **10**, 1737-1744.
17. J.-P. Zhang, A.-X. Zhu, R.-B. Lin, X.-L. Qi and X.-M. Chen, *Adv. Mater.*, 2011, **23**, 1268-1271.
18. G. Akiyama, R. Matsuda, H. Sato, A. Hori, M. Takata and S. Kitagawa, *Micropor. Mesopor. Mater.*, 2012, **157**, 89-93.
19. (a) H. Reinsch, M. A. van der Veen, B. Gil, B. Marszalek, T. Verbiest, D. de Vos and N. Stock, *Chem. Mater.*, 2012, **25**, 17-26; (b) M. F. D. Lange, C. P. Ottevanger, M. Wiegman, T. J. H. Vlugt, J. Gascon and F. Kapteijn, *CrystEngComm.*, 2015, **17**, 281-285; (c) B. Q. Tan, Y. S. Luo, X. H. Liang, S. F. Wang, X. N. Gao, Z. G. Zhang and Y. T. Fang, *Cryst. Growth Des.*, 2020, **20**, 6565-6572.

20. J. Canivet, J. Bonnefoy, C. Daniel, A. Legrand, B. Coasne and D. Farrusseng, *New J. Chem.*, 2014, **38**, 3102-3111.
21. H. Furukawa, F. Gandara, Y. B. Zhang, J. Jiang, W. L. Queen, M. R. Hudson and O. M. Yaghi, *J Am Chem Soc.*, 2014, **136**, 4369-4381.
22. N. Ko, J. Hong, S. Sung, K. E. Cordova, H. J. Park, J. K. Yang and J. Kim, *Dalton Trans.*, 2015, **44**, 2047-2051.
23. J. R. Álvarez, R. A. Peralta, J. Balmaseda, E. G. Zamora and I. A. Ibarra, *Inorg. Chem. Front.*, 2015, **2**, 1080-1084.
24. S. Ø. Ødegaard, B. Bouchevreau, K. Hylland, L. Wu, R. Blom, C. Grande, U. Olsbye, M. Tilset and K. P. Lillerud, *Inorg. Chem.*, 2016, **55**, 1986-1991.
25. R. G. AbdulHalim, P. M. Bhatt, Y. Belmabkhout, A. Shkurenko, K. Adil, L. J. Barbour and M. Eddaoudi, *J. Am. Chem. Soc.*, 2017, **139**, 10715-10722.
26. (a) S. Dissegna, R. Hardian, K. Epp, G. Kieslich, M. V. Coulet, P. Llewellyn and R. A. Fischer, *CrystEngComm.*, 2017, **19**, 4137-4141; (b) S. Waitschat, D. Fröhlich, H. Reinsch, H. Terraschke, K. A. Lomachenko, C. Lamberti, H. Kummer, T. Helling, M. Baumgartner, S. Henningerb and N. Stock, *Dalton Trans.*, 2018, **47**, 1062-1070.
27. (a) S. Kayal, A. Chakraborty and H. W. B. Teo. *Mater. Lett.*, 2018, **221**, 165-167; (b) N. Hanikel, M. S. Prevot, F. Fathieh, E. A. Kapustin, H. Lyu, H. Wang, N. J. Diercks, T. G. Glover and O. M. Yaghi, *ACS Cent. Sci.*, 2019, **5**, 1699-1706.
28. S. M. T. Abtab, D. Alezi, P. M. Bhatt, A. Shkurenko, Y. Belmabkhout, H. Aggarwal, Ł. J. Weseliński, N. Alsadun, U. Samin, M. N. Hedhili and M. Eddaoudi, *Chem.*, 2018, **4**, 94-105.
29. Y.-Z. Zhang, T. He, X.-J. Kong, X.-L. Lv, X. Q. Wu and J.-R. Li, *ACS Appl Mater Interfaces.*, 2018, **10**, 27868-27874.
30. (a) K. M. Hunter, J. C. Wagner, M. Kalaj, S. M. Cohen, W. Xiong and F. Paesani, *J. Phys. Chem. C.*, 2021, **125**, 12451-12460; (b) M.-Z. Gao, J. Wang, Z.-H. Rong, Q. Shi and J.-X. Dong, *RSC Adv.*, 2018, **8**, 39627-39634.
31. (a) K. Yanagita, J. Hwang, J. A. Shamim, W. L. Hsu, R. Matsuda, A. Endo, J. J. Delaunay and H. Daiguji, *J. Phys. Chem. C.*, 2019, **123**, 387-398; (b) S. Fei, A. Alizadeh, W. L. Hsu, J. J. Delaunay and H. Daiguji, *J. Phys. Chem. C.*, 2021, **125**, 26755-26769; (c) M. Wickenheisser, A. Herbst, R. Tannert, B. Milow, C. Janiak, *Micropor. Mesopor.Mater.*, 2015, **215**, 143-153.

32. Z.-J. Chen, P.-H. Li, X. Zhang, P. Li, M. C. Wasson, T. Islamoglu, J. F. Stoddart and O. K. Farha, *J. Am. Chem. Soc.*, 2019, **141**, 2900-2905.
33. J. S. Lee, J. W. Yoon, P. G. M. Mileo, K. H. Cho, J. Park, K. Kim, H. Kim, M. F. de Lange, F. Kapteijn, G. Maurin, S. M. Humphrey and J. S. Chang, *ACS Appl. Mater. Interf.*, 2019, **11**, 25778-25789.
34. N. C. Burtch, I. M. Walton, J. T. Hungerford, C. R. Morelock, Y. Jiao, J. Heinen, Y.-S. Chen, A. A. Yakovenko, W. Xu, D. Dubbeldam and K. S. Walton, *Nat. Chem.*, 2019, **12**, 186-192.
35. (a) S. Leubner, R. Staglich, J. Franke, J. Jacobsen, J. Gosch, R. Siegel, H. Reinsch, G. Maurin, J. Senker, P.-G. Yot, and N. Stock, *Chem. -Eur. J.*, 2020, **26**, 3877-3883; (b) T. Stassin, S. Waitschat, N. Heidenreich, H. Reinsch, F. Pluschkell, D Kravchenko, J. Marreiros, I. Stassen, J. V. Dinter, R. Verbeke, M.l Dickmann, W. Egger, I.Vankelecom, D. D. Vos, R. Ameloot and N. Stock, *Chem. Eur. J.*, 2020, **26**, 10841-10848.
36. C. Schlüsener, D. N. Jordan, M. Xhinovci, T. J. M. M. Ntep, A. Schmitz, B. Giesen and C. Janiak, *Dalton Trans.*, 2020, **49**, 7373-7383.
37. A. Kuznicki, G. R. Lorzing and E. D. Bloch, *Chem. Commun.*, 2021, **57**, 8312-8315.
38. M. Solovyeva, I. Krivosheeva, L. Gordeeva and Y. Aristov, *Energies*, 2021, **14**, 3586-3601.
39. M. P. Irigaray, G. Beobide, S. Calero, O. Castillo, I. D. Silva, J. J. G. Sevillano, A. Luque, S. P. Yáñez and L. F. Velascog, *Inorg. Chem. Front.*, 2021, **8**, 4767-4779.
40. W. Gong, H.-M. Xie, K. B. Idrees, F. A. Son, Z.-J. Chen, F.-R. Sha, Y. Liu, Y. Cui and O. K. Farha, *J. Am. Chem. Soc.*, 2022, **144**, 1826-1834.
41. Z.-Y. Lu, J.-X. Duan, L. Du, Q. Liu, N. M. Schweitzerd and J. T. Hupp, *J. Mater. Chem. A.*, 2022, **10**, 6442-6447.